Additive Manufacturing 59 (2022) 103129

Contents lists available at ScienceDirect

Additive Manufacturing

journal homepage: www.elsevier.com/locate/addma

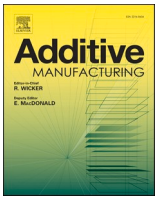

Material extrusion thermal model mapped across polyetheretherketone isothermal and continuous cooling transformation charts

Cleiton André Comelli [a,*], Nan Yi [a], Richard Davies [a], HenkJan van der Pol [b], Oana Ghita [a]

[a] University of Exeter, College of Engineering, Mathematics and Physical Sciences, Harrison Building, Streatham Campus, North Park Road, EX4 4QF Exeter, UK
[b] Bond High Performance 3D Technology, Institutenweg 50, Enschede 7521 PK, the Netherlands

ARTICLE INFO

Keywords:
PEEK
MEX
Crystallisation
DSC
FSC

ABSTRACT

This study provides an insight into the polyetheretherketone (PEEK) crystallinity progression throughout the material extrusion (MEX) additive manufacturing process as a function of time and temperature, comparing it with the isothermal and continuous cooling transformation charts created over a wide range of isothermal crystallisation temperatures and constant cooling rates. The isothermal and non-isothermal crystallisation kinetics were explored using Differential Scanning Calorimetry (DSC) and Fast Scanning Calorimetry (FSC). The half-time, onset and ending of crystallisation were obtained for isothermal crystallisation temperatures between 150 °C and 330 °C, while the crystallisation under constant cooling was obtained using rates between − 0.5 K s^{-1} and − 45 K s^{-1}. The results were used to draw the Continuous Cooling Transformation (CCT) and the Time-Temperature Transformation (TTT) diagrams and calculate the Avrami numbers using the parallel Avrami model. These results were then compared to the degree of crystallinity as a function of time and temperature for the MEX process. To evaluate the crystallisation within the MEX process a 1D transient transfer heat model was used to obtain the printing thermal profile, which was replicated using the FSC technique. The results showed that for the MEX printing process, the crystallisation usually is a product of a combination of rapid cooling and heating processes followed by periods of greater thermal stability which, depending on the nature of the process, can approach a quasi-isothermal crystallisation process. By superimposing the process thermal profile on the TTT and CCT diagrams and comparing the crystallinity values measured from each point in the thermal profile, it was possible to understand the crystallinity evolution and the remelting of the build surface promoted by the subsequent printed layers.

1. Introduction

The use of high-performance thermoplastic materials has increased considerably as advanced applications appear in the most diverse areas of engineering. In this context, the family of polyaryletherketones (PAEKs) stands out thanks to its exceptional mechanical properties associated with excellent heat resistance and chemical stability [1–4]. Polyetheretherketone (PEEK) is part of the PAEKs family and shares the excellent properties of these polymers, its structure is semi-crystalline and typically has a degree of crystallinity close to 35% [3]. However, crystallinity can vary considerably, being strongly influenced by the thermal cycle to which PEEK is exposed during its processing [5].

Additive manufacturing (AM) refers to a series of production techniques based on the joining of material, usually in layers, that allow the production of parts directly from a digital 3D model, especially parts with high complexity, often difficult to be produced by traditional manufacturing methods [6,7]. Because of its potential, AM techniques have gained prominence among the processing techniques that can be used for the manufacture of PEEK parts [3], [8–11].

Among the AM processes, material extrusion (MEX) is a very popular option, since it offers great versatility and relatively low running costs. Initially, it was widely used for the manufacture of visual parts, assembly tests or educational models and currently, the technique has gained space in the manufacture of functional parts [12]. MEX is based on selective material extrusion through a computer-controlled nozzle, producing the parts layer upon layer and offering compatibility with a great variety of printing materials, including PEEK and other high-performance materials [13–17].

* Corresponding author.
E-mail addresses: cleiton.comelli@gmail.com (C.A. Comelli), n.yi@exeter.ac.uk (N. Yi), richard.davies@exeter.ac.uk (R. Davies), hj.vanderpol@bond3d.com (H. van der Pol), o.ghita@exeter.ac.uk (O. Ghita).

https://doi.org/10.1016/j.addma.2022.103129
Received 21 June 2022; Received in revised form 16 August 2022; Accepted 5 September 2022
Available online 7 September 2022

Despite the advantages of AM to produce parts, especially when high-performance polymers are used, there are still several challenges associated with such processes. Semi-crystalline polymers, such as PEEK 450 G™, are increasingly gaining attention since they can provide excellent mechanical properties in high-temperature environments associated with chemical and wear resistance. However, as with any other semi-crystalline polymer when compared with amorphous ones, PEEK is more prone to geometrical distortions such as warpage and thermal shrinkage, which can be explained by the ordering process of long polymeric chains during the crystallization process. Moreover, depending on the temperature conditions, PEEK may also present a very fast crystallisation rate which is a phenomenon that, if not well understood and predicted during the manufacture of the part, can result in considerable geometric distortions [17–20].

Vaes and Van Puyvelde (2021), provided a broad overview of the MEX processing of semi-crystalline polymers, focusing on processing parameters and feedstock modifications with fillers and blends and their effects on crystallinity, microstructure, mechanical performance and part quality. The authors explain the limitations imposed by the excessive shrinkage during crystallization for some polymers, such as polypropylene (PP), which is commercially modified to suppress crystallization and enhance printability. Other specific phenomena related to semi-crystalline polymers including insufficient melting and self-nucleation, orientational effects, flow-induced crystallization and interlayer adhesion are broadly discussed. Also, the effect of excessive cooling, MEX repeated heating cycles boost on crystallinity, and the shear-induced crystallization are reported for polylactic acid (PLA) parts. Polyamides (PA), polycaprolactone (PCL) and other polyesters are also covered in the review and finally high-performance polymers, including PEEK [21].

The PEEK crystallisation has been explored by several authors [5], [22–29]. A comprehensive work regarding isothermal crystallisation was presented by J. Seo et al. [24]. The authors investigated the influence of molecular weight on the isothermal crystallisation of PEEK 150 G, 450 G™ and 650 G using a combination of DSC and FSC to cover a wide range of temperatures (158 °C to 336 °C), also providing an Avrami fitting to the crystallisation curves.

A time-temperature transformation (TTT) chart was also provided showing the half-time crystallisation analysis and a shift in the maximum crystallisation rate to lower temperature with an increase in molecular weights (MW) (223 °C for PEEK 150 G, 220 °C for PEEK 450 G™ and 217 °C for PEEK 650 G). The authors reported a longer crystallisation time and lower absolute crystallinity for higher MW [24], explained by the lower mobility provided by longer chains, which increases the complexity of the chain folding and crystallisation.

Isothermal and non-isothermal crystallisation was also explored by Bas et al. using DSC, density analysis, and wide-angle X-ray scattering (WAXS). The Continuous Cooling Transformation (CCT) and the Time-Temperature Transformation (TTT) diagrams were obtained by the authors, showing competition between the nucleation process and the spherulite growth process, with low temperatures favouring the nucleation processes while for higher temperatures, the growth process prevailed. For non-isothermal processes, higher cooling rates showed a decrease in the crystallisation ability of PEEK [29].

Despite the relatively large number of studies addressing PEEK crystallisation available in the literature, most of the works focussed on the isothermal or non-isothermal analysis of crystallisation in isolation, without linking it to actual production processes, where a combination of different cooling and heating rates is more common [22,23], [30,31]. Furthermore, since molecular diffusion and crystallisation are processes directly dependent on temperature and time, the evaluation of PEEK crystallisation in any manufacturing process depends on the knowledge of the temperature profile to which the material is exposed [22,23], [32,33].

For MEX processes, obtaining the material temperature as a function of time at a given stage during the filament deposition can become a complex task. The use of thermocouples or IR cameras is usually the chosen method, however, thermocouples can only measure the temperature of a static point in the printed part, normally at the interface between layers. Thermocouples usually present considerable thermal mass and size and may interfere with the printing process, while IR thermometers can only measure the surface temperature and rely on a good calibration to produce trustable results [34–36]. Vanaei et al., for example, obtained the MEX process thermal profile for PLA using thermocouples and IR cameras, noting differences and suggesting that the results obtained using the IR camera could be optimized with the results obtained from the thermocouples [36].

Although they also have limitations, mathematical thermal models can also be used and may allow estimating the local temperature variation at any point of the extruded material, which would be impossible using other methods. For additive manufacturing processes based on MEX, some thermal models have already been suggested and their application allows obtaining process thermal profiles as a function of key parameters, such as extrusion speed or temperature [32], [37].

In the case of the MEX process, the thermal profile for a certain point is highly influenced by the superposition of fused filaments which causes a large variation in the local temperature, and this influence, at the same point, becomes milder as extra layers are produced. This intrinsic characteristic of the process makes the temperature profile largely non-isothermal, for regions closer to the filament deposition spot, with temperatures fluctuations that are damped by the next layers until a cool-down phase takes place, at this time, being more influenced by the build platform, chamber or ambient temperature [32,33], [36].

Vaes et al. proposed an interesting method to evaluate the crystallinity evolution for MEX [33]. The authors used PA to manufacture a thin-walled geometry (composed of a single filament), varying the extrusion temperature, build platform temperature and printing speed. An IR camera was used to obtain the thermal history during the printing process and, subsequently, the resulting thermal profile was mimicked using FSC to evaluate the evolution of crystallinity in the tenth and fortieth layer of the thin wall. In each of the layers replicated in the FSC, the authors measured the crystallinity at three different points, the first being after the overlap of the subsequent layer, the second at the end of the thermal profile measured by the IR camera, and finally at the end of the process. The results showed that the extrusion temperature and print speed had a minor influence on the resulting crystallinity, which was instead, strongly affected by the build platform temperature. Also, it is interesting to notice that the same methodology could be used for other polymers as well, including high-performance ones, such as PEEK.

Schiavone et al. investigated the isothermal and non-isothermal crystallisation of PLA, in addition to the influence of variations in the thermal profile in the MEX process, evaluating the influence of the time interval between layers through an analysis method based on finite element simulation (FEM). According to the authors, different deposition times of layers resulted in significant differences in the thermal profiles obtained, with the addition of new filaments promoting a heating and cooling cycle, which stimulates crystallisation that develops in a step pattern, according to the sequence of addition of new filaments [38].

Zeng et al., also using numerical finite element analysis, developed a model to predict the thermal profile of the MEX process for acrylonitrile butadiene styrene (ABS). The model was validated using micro thermocouples inserted between the first layer and the build platform and between the second and third layers; the results proved to have good accuracy [18].

Most of the works dedicated to the analysis of the thermal profile of the MEX process are focused on lower melting point polymers, some amorphous. In terms of high-performance polymers, the work developed by C. Basgul et al. proposed a thermal model using PEEK as the printing material. The authors developed a unidirectional (1D) transient heat transfer model to predict the temperatures of the layers and interlayer regions during the printing of PEEK parts and can be used to generate

Table 1
PEEK 450 G™ properties [1].

Properties	Conditions	Test method	Units	Typical value
Tensile Strength	Yield, 23 °C	ISO 527	MPa	98
Tensile modulus	23 °C	ISO 527	GPa	4
Melting point	–	ISO 11357	°C	343
Glass Transition (Tg)	Onset	ISO 11357	°C	143
Density	Crystalline	ISO 1183	g cm^{-3}	1.30

realistic MEX process thermal profiles [32].

As the intermolecular diffusion and neck growth between filaments is a function of temperature and directly influences the interlayer adhesion, being stronger above the crystallisation temperature for semicrystalline polymers and above the glass transition temperature for amorphous polymers. The detailed understanding of the thermal cycle of the MEX process and its relationship with the crystallisation process becomes fundamental for the understanding of the process parameters needed to obtain a satisfactory adhesion of the filaments [36].

In this context, the present work combines numerical thermal profiles of the MEX process for PEEK printing, obtained using the thermal model proposed by C. Basgul et al., with the crystallisation behaviour suggested by the transformation diagrams obtained for PEEK 450 G™ focusing especially on the interaction between the build surface and the material addition during the layer deposition to explain what is desirable in a thermal profile to obtain good interlayer adhesion and, consequently, good mechanical performance.

2. Materials and methods

2.1. Material

Victrex™ PEEK 450 G™ was used for this study. The material was supplied in rods by Bond High Performance 3D Technology. The main properties are presented in Table 1.

2.2. Thermal and crystallisation analyses

A DSC (DSC 3 - Mettler Toledo, UK) and an FSC (Flash DSC 2 + - Mettler Toledo, UK) were used for the thermal analysis. For DSC, the size of the samples ranged from 8 to 10 mg and the initial characterization of the material was performed to measure the cold crystallisation temperature (Tcc), the glass transition temperature (Tg), the melting temperature (Tm), and the crystallisation temperature (Tc). This was achieved by initially heating the material from the solid state to the temperature of 400 °C, using a heating rate of 10 K min^{-1}, followed by a cooling (−10 K min^{-1}) to the temperature of 30 °C. For all DSC experiments, a flow of 50 ml min^{-1} of nitrogen was used.

The resulting thermogram was used to select the temperatures for the isothermal crystallisation analysis using the DSC and FSC. Fig. 1 shows the respective zones explored on DSC (blue and red) and FSC (yellow).

For the crystallisation analysis, the lower crystallisation rate regions, which are located at the beginning and the end of the temperature range, (shown in Fig. 1 by the blue and red regions) were explored using the DSC. For the higher temperatures (T_c > 310 °C), the samples were cooled from the molten state, and for the lower temperatures (T_c < 155 °C), amorphous samples were used, being heated from the solid state.

The fast cooling rates offered by the FSC allow the analysis of the crystallisation of fast crystallizing polymers, such as PEEK 450 G™ in the temperature ranges in which the crystallisation rate is maximum (Yellow region in Fig. 1), therefore, the equipment was used for the detailed study of the crystallisation of the material under these conditions. In addition, the study of non-isothermal crystallisation and the simulation of the thermal profile corresponding to the MEX process were also achieved using this technique. The experiments used a UFS1 type sensor, which offers heating rates from 0.1 to 50′000 K s^{-1} and cooling rates from 0.1 to 4′000 K s^{-1}. A sample of the material with a mass of 260 ng was prepared with the aid of a microtome and a razor blade and placed precisely in the centre position of the sensor.

The sample mass was calculated using the superposition of the FSC and DSC scanning rates, which allows for generating samples with similar crystallinity, since similar cooling rates are applied to both, DSC and FSC samples [39]. In this method, if the crystallinity is similar, by definition, both specific enthalpies of melting should be equal, and the mass of the sample can be estimated by the following formula:

$$m, FSC = \frac{\Delta H_{m,FSC}}{\Delta H_{m,DSC}} * m, DSC \quad (1)$$

Where $\Delta H_{m,FSC}$ and $\Delta H_{m,DSC}$ are the melting enthalpies, measured by the FSC and DSC, respectively, and $m,\ FSC$ and $m,\ DSC$ are the sample masses.

The FSC technique can present thermal lag effects at fast heating rates that increase with increasing sample size and heating rates. According to Poel et al., for a heating rate of 1000 K s^{-1} (which was used

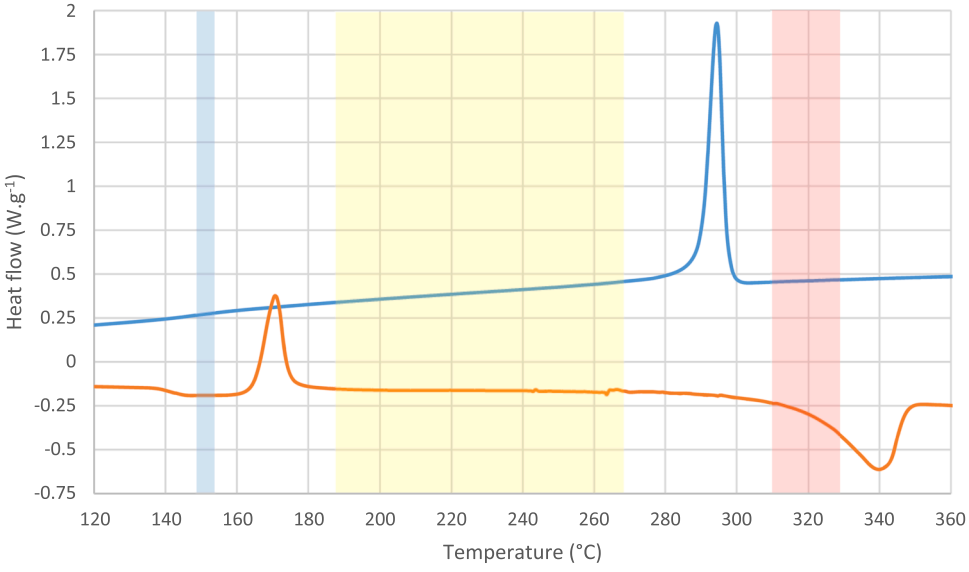

Fig. 1. DSC thermogram of the PEEK 450 G™ (amorphous sample) showing the temperature ranges evaluated in blue, yellow and red.

Table 2
Isothermal temperatures and times used for thermal crystallisation analysis. DSC temperatures are presented in bold and FSC are presented in italics. The cold crystallisation is represented by "cc", and the crystallisation from the melt is represented by "mc".

Temp. (°C)	Time (min)	Temp. (°C)	Time (min)	Temp. (°C)	Time (min)	Temp. (°C)	Time (min)
152.5 (cc)	360 min	*217.5*	60 s	*237.5*	60 s	*270.0*	60 s
155.0 (cc)	180 min	*220.0*	60 s	*240.0*	60 s	**310.0 (mc)**	180 min
190.0	60 s	*222.5*	60 s	*242.5*	60 s	**315.0 (mc)**	240 min
200.0	60 s	*225.0*	60 s	*245.0*	60 s	**320.0 (mc)**	240 min
205.0	60 s	*227.5*	60 s	*247.5*	60 s	**325.0 (mc)**	440 min
210.0	60 s	*230.0*	60 s	*250.0*	60 s	**327.5 (mc)**	720 min
212.5	60 s	*232.5*	60 s	*255.0*	60 s	**330.0 (mc)**	720 min
215.0	60 s	*235.0*	60 s	*260.0*	60 s		

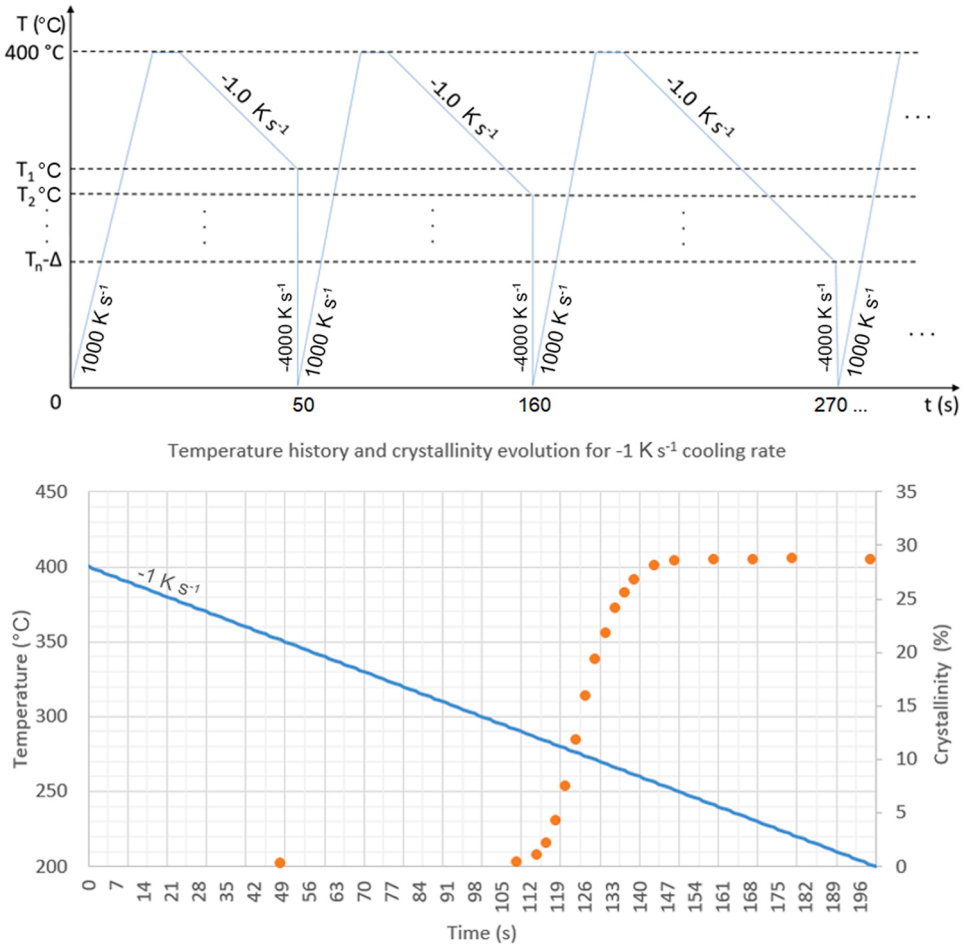

Fig. 2. FSC thermal cycle and sample crystallisation curve showing the set of points measured for the cooling rate of − 1 K s^{-1}. The same procedure was repeated for each of the cooling rates tested.

throughout the melting analysis in this work) and a sample size of 285 ng (which is very close to the 260 ng used here), a variation of 0.8 °C on melting onset temperature can be expected [39]. However, as the focus of the study is on understanding the degree of crystallisation, the 0.8 °C thermal lag is not expected to significantly impact the results. For the non-isothermal analysis, the maximum cooling rate used was − 45 K s^{-1}, and therefore, thermal lag was negligible.

2.2.1. Isothermal crystallisation and Time-Temperature-Transformation chart

The PEEK 450 G™ crystallisation under isothermal conditions was explored for a wide range of temperatures. The initial experiments were carried out in the DSC and were divided into two groups, hot crystallisation and cold crystallisation. For hot crystallisation, six isothermal temperature levels were evaluated by rapid cooling from the molten state, using a cooling rate of − 100 K min^{-1}. For the cold crystallisation, two isothermal temperature levels were evaluated by heating samples from the amorphous state, using a heating rate of 300 K min^{-1}.

The eight temperatures evaluated using the DSC were complemented by 23 measurements performed using the FSC, all from the molten state, taking advantage of the high cooling rate available to avoid crystallisation before the target temperature was reached. Table 2 shows the temperatures (DSC in bold) together with the isothermal crystallisation time used for each one.

The thermal cycle applied for the temperatures tested with FSC consisted of heating the sample to the molten state (400 °C), a temperature at which the sample was held for one second before being rapidly cooled, using a cooling rate of @ −4000 K s^{-1}, to the target isothermal

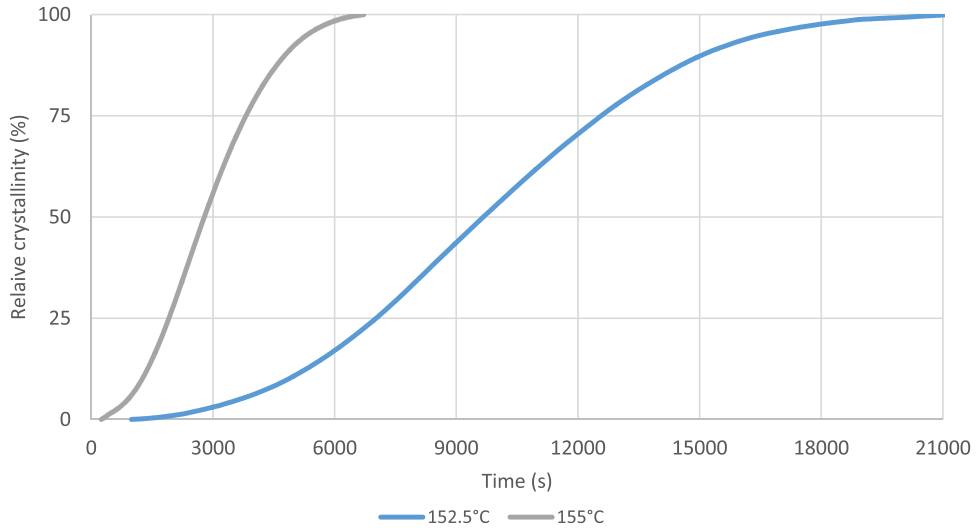

Fig. 3. Relative crystallinity curves obtained by cold crystallisation analysis on DSC.

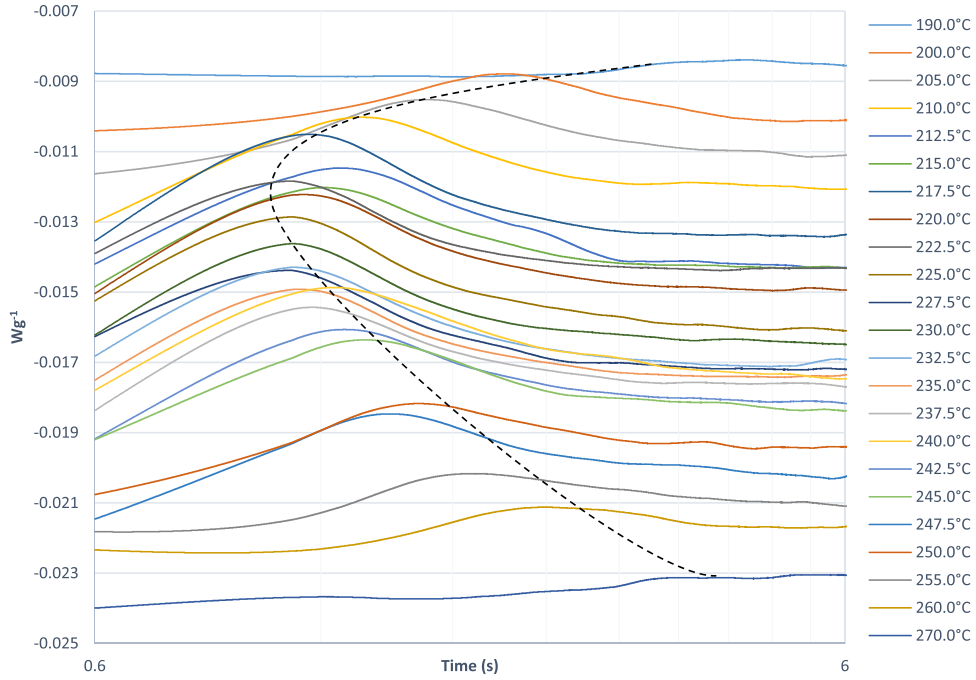

Fig. 4. FSC crystallisation curves from 190 °C (top) to 270 °C (bottom).

crystallisation temperature, at which it was maintained for 60 s and then rapidly cooled to 30 °C, using a cooling rate of − 4000 K s^{-1}.

After crystallisation at each of the isothermal temperature levels, the thermograms of the resulting exothermic curves were plotted as a function of time. By integrating the curves, the relative crystallinity chart for each temperature was obtained.

2.2.2. *Non-isothermal crystallisation and continuous cooling transformation chart*

The analysis of non-isothermal crystallisation was performed through the continuous cooling of the polymer from the molten state using different cooling rates. For each cooling rate, the absolute crystallinity in addition to the onset and end of the crystallisation process was measured. To achieve this, the experiments were performed using the FSC, the test consisted in heating the sample to the molten state (@400 °C) and cooling it to multiple target temperatures for every cooling rate tested (see Appendix A).

After each target temperature was reached, the sample was quickly cooled (−4000 K s^{-1}) to 30 °C and subsequently heated to 400 °C to measure the crystallinity formed up to that point. With the set of all crystallinities measured for each cooling rate, graphs of relative crystallinity were plotted. Fig. 2 schematically shows the thermal cycle used and a sample curve with the different points measured for a cooling rate of − 1 K s^{-1}.

2.3. *Crystallisation process fitting using parallel Avrami*

The crystallisation curves were fitted using the parallel Avrami model, this model was used by C. Velisaris et al., and modified versions are also proposed in the literature [40]. For this study, the model was used following the fitting method proposed by J. Seo et al. [24]. For the parallel Avrami model, two competitive processes of nucleation and

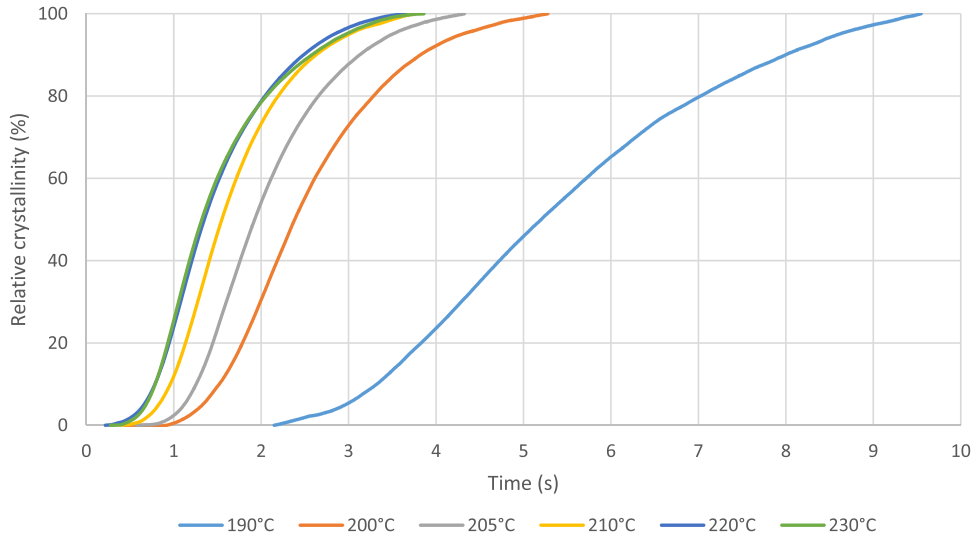

Fig. 5. FSC crystallisation curves from 190 °C to 230 °C.

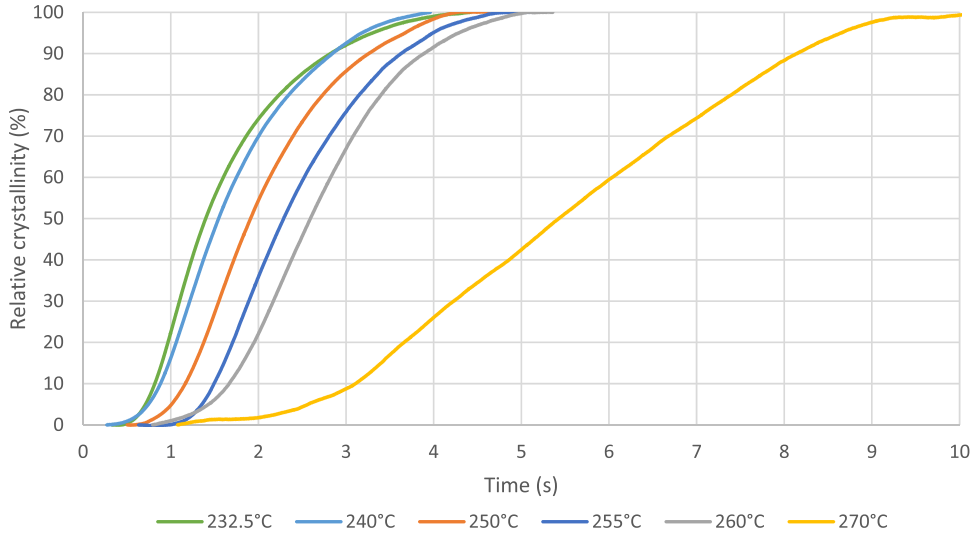

Fig. 6. FDSC crystallisation curves from 232.5 °C to 270 °C.

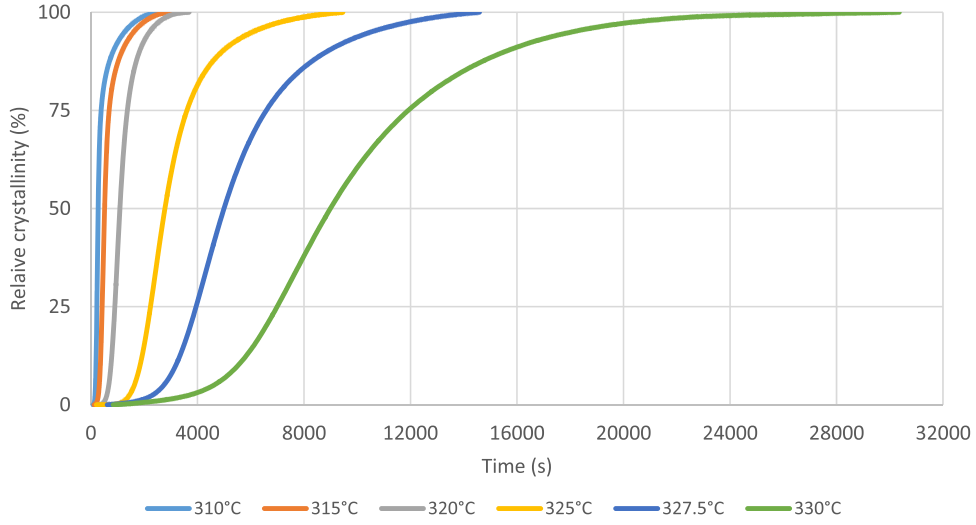

Fig. 7. DSC crystallisation curves from 310 °C to 330 °C.

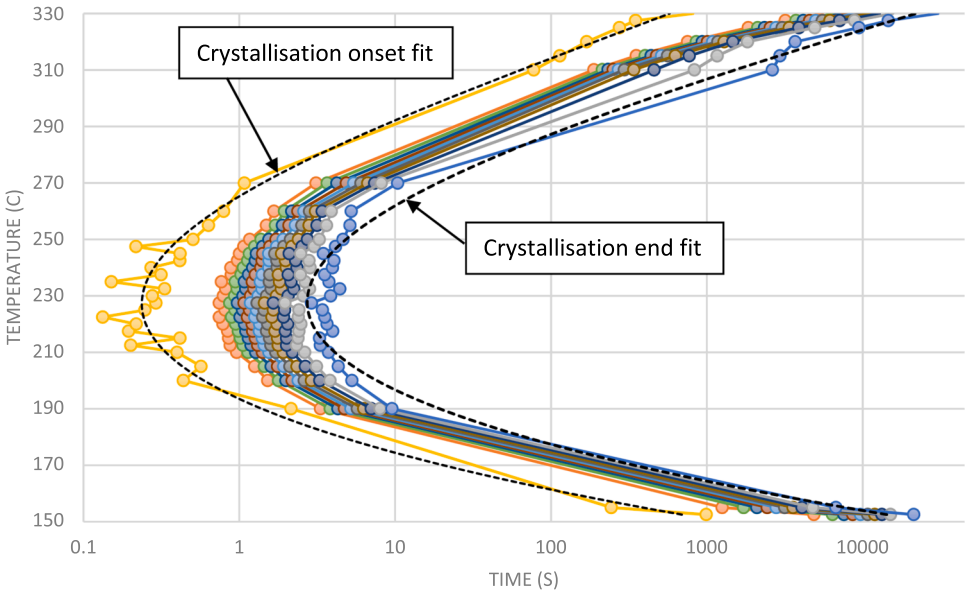

Fig. 8. TTT diagram for PEEK 450 G™.

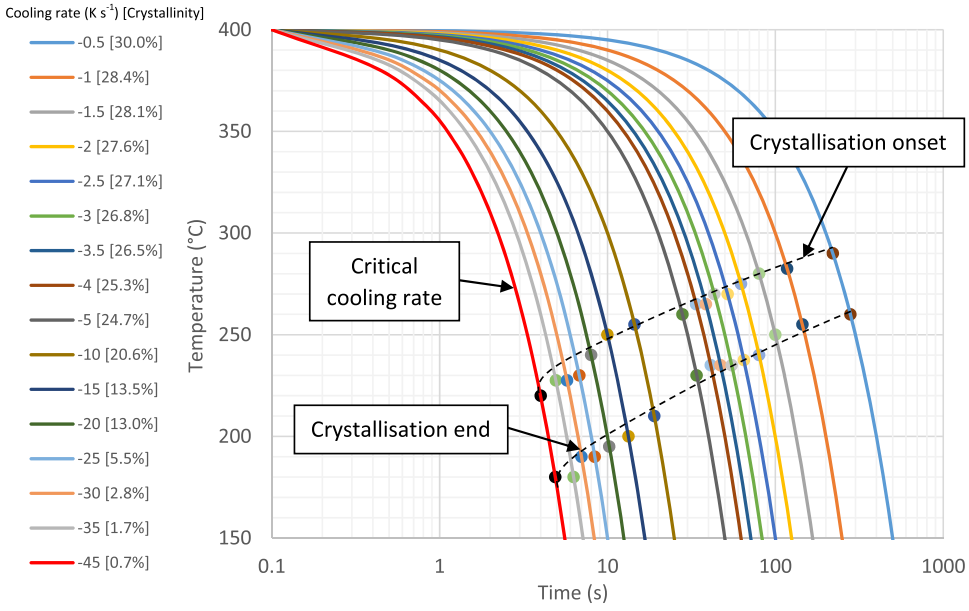

Fig. 9. CCT diagram for PEEK 450 G™.

crystal growth are considered through a linear combination of two Avrami equations, given by

$$\frac{Xvc}{Xvc\infty} = wp * [1 - \exp(-kp * t^{np})] + ws * [1 - \exp(ks * t^{ns})] \quad (2)$$

With:

$$wp + ws = 1 \quad (3)$$

Where *kp* and *ks* represent the crystallisation rate constant for the primary and secondary mechanisms, *np* and *ns* are the Avrami exponents for the primary mechanism and secondary mechanism, *t* stands for time, *wp* and *ws* are the weight factors while *Xvc* is the volume fraction crystallinity and *Xv*∞ is the equilibrium volume fraction crystallinity.

2.4. Printing process simulation on FSC and crystallinity evolution

The model proposed by C. Basgul et al. was used to generate thermal profiles of the MEX printing process with the thermal properties of PEEK 450 G™. It is a one-dimensional model of transient heat transfer that allows generating the thermal profiles through which the feedstock is subjected during the MEX process. The model assumes a uniform thermal distribution in the deposited layer and parameters such as build platform temperature, extrusion temperature, build chamber temperature, layer time, layer thickness and number of layers can be varied.

In the present study, the extrusion temperature and the build surface temperature were considered constant during the process and the thermal profile for a single first layer was obtained for two different temperatures of the build platform (150 °C and 250 °C). The same process was applied to obtain the thermal profile corresponding to multiple layers with layer times of 20 or 60 s. The extrusion temperature

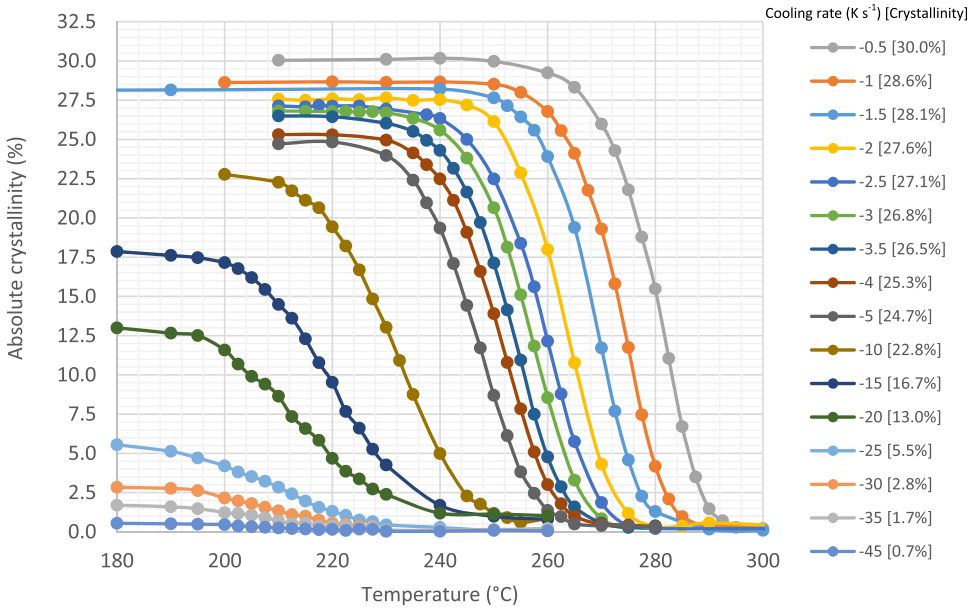

Fig. 10. Crystallinity as a function of temperature and cooling rate for PEEK 450 G™.

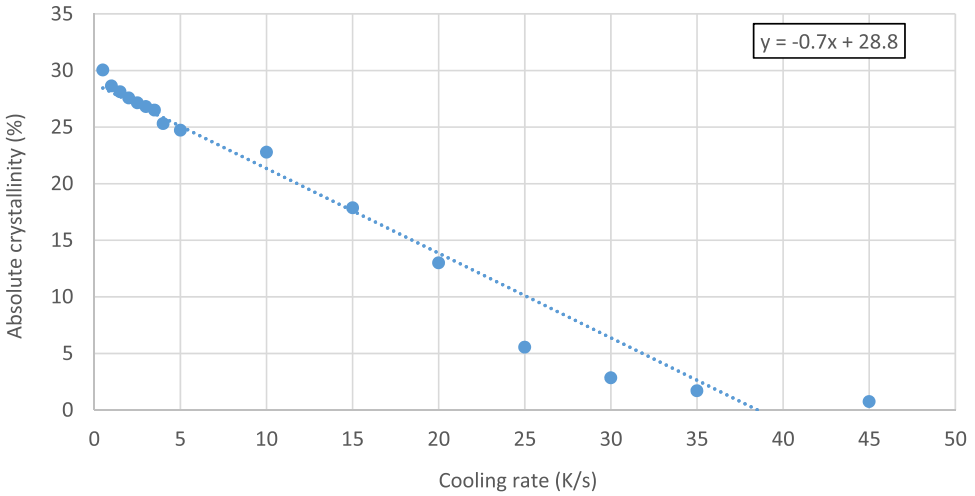

Fig. 11. Absolute crystallinity as a function of cooling rate for PEEK 450 G™.

was 400 °C with a chamber temperature of 100 °C and a layer thickness of 0.5 mm throughout the process. The PEEK properties used in the simulation were thermal conductivity of 0.32 W K m^{-1}, the specific heat capacity of 1957 J (kg K)$^{-1}$, and density of 1300 kg m^{-3} [1], [32].

Crystallinity evolution was measured along with the single and multi-layer thermal profiles, by splitting them into 37 and 18 points, respectively, and measuring the crystallinity for each point. The results were used to compare with the transformation diagrams, helping to understand the remelting effect promoted by subsequent layers on crystallinity evolution.

3. Results

3.1. Crystallisation analysis

3.1.1. Isothermal crystallisation and TTT diagram

Using amorphous samples and the DSC to evaluate the first region (blue – Fig. 1) which corresponds to the cold crystallisation, the isothermal crystallisation for 152.5 °C and 155 °C was achieved resulting in two crystallisation curves shown in Fig. 3.

For the middle region (yellow – Fig. 1), the crystallisation rate increased substantially and the analysis was performed by FSC, the 23 temperatures evaluated resulted in a set of crystallisation curves with longer crystallisation times at both ends of the temperature range, while the highest crystallisation rate was reached in the middle, approximately at the isothermal temperature of 230 °C. The set of curves showed a C shape pattern, as shown in Fig. 4.

The main relative crystallinity curves obtained from the crystallisation curves are shown in Figs. 5 and 6.

For the higher temperatures (red region), crystallisation was again evaluated using the DSC, cooling the sample from the molten state, the resulting crystallisation curves are shown in Fig. 7.

With the relative crystallisation curves, the onset and end of crystallisation can be represented in the form of a TTT Diagram. 10% increments were plotted along with the measured maximum and minimum values and the curves were fitted using a third-order polynomial equation, as shown in Fig. 8.

The highest crystallisation rate was observed between 220 °C and 230 °C, values that are in line with what was previously reported in the literature [24].

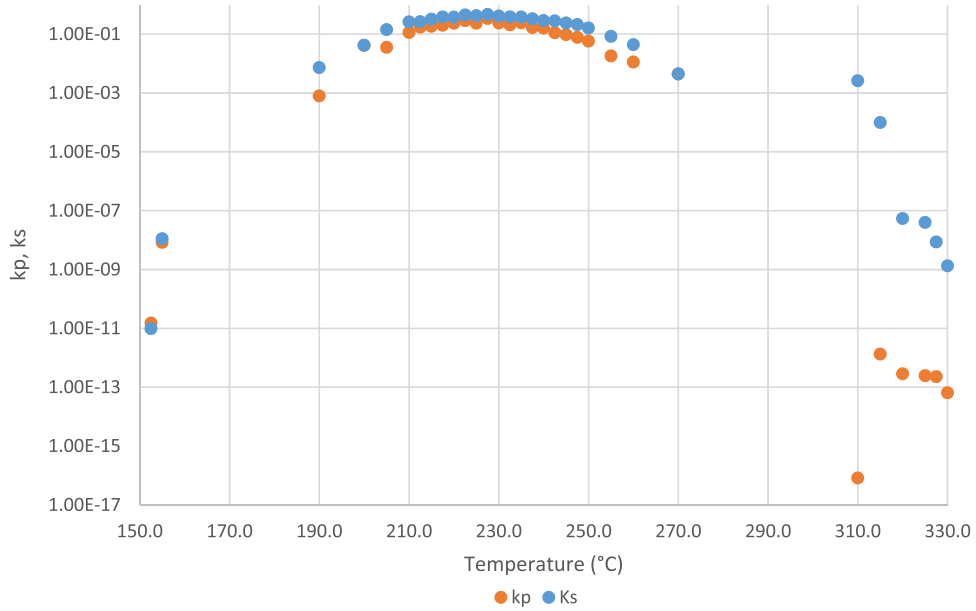

Fig. 12. Crystallisation rate constants (K_s and K_p) for PEEK 450 G™.

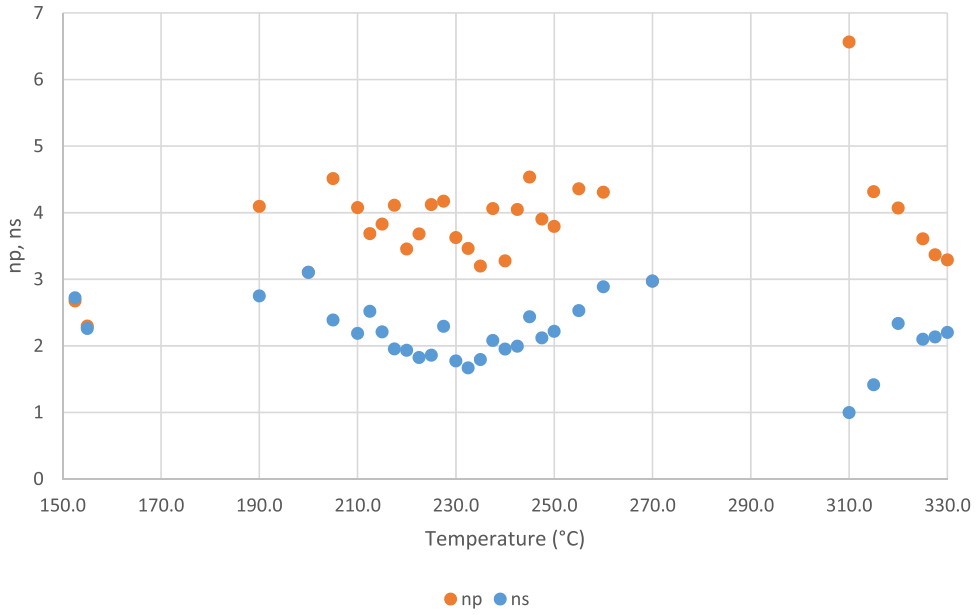

Fig. 13. Parallel Avrami exponents (*ns* and *np*) for PEEK 450 G™.

3.1.2. Non-isothermal crystallisation and CCT diagram

The results of the non-isothermal crystallisation analysis present (for each cooling rate) the onset and end of the crystallisation process in addition to the absolute crystallinity, as shown in Fig. 9. The critical cooling rate is shown by the red line, above this cooling rate (left region of the graph in Fig. 9) the crystallinity sits below 0.7%.

The lower cooling rates resulted in higher degrees of absolute crystallinity, with the rate of $-0.5\ \mathrm{K\ s^{-1}}$ reaching a crystallinity value of 30.0%. As the cooling rate is increased, the temperatures associated with the onset and end of crystallisation are reduced as well as the absolute crystallinity, which, at the lower end (cooling rate of $-45\ \mathrm{K\ s^{-1}}$), corresponded to only 0.7%. This behaviour becomes even clearer when the crystallinity is plotted as a function of time for each of the cooling rates used, as shown in Fig. 10.

The absolute crystallinity when plotted as a function of the cooling rate can be fitted using a linear equation which can be used to estimate the resulting crystallinity as a function of the cooling rate, as shown in Fig. 11.

3.1.3. Crystallisation fitting using parallel Avrami model

The crystallisation curves were fitted using the parallel Avrami model and the values obtained for the exponents at each temperature were plotted as shown in Fig. 12. For the exponent's *Ks* and *Kp*, an inverted bell shape can be observed, with values closer to 1.0 for faster crystallisation temperatures.

The same procedure was repeated for the values obtained for the exponent *ns* and *np* and are shown in Fig. 13. It is possible to observe that higher values, mostly between 3 and 4, were obtained for *np* while lower values (closer to 2) were obtained for *ns*. The interpretation of these exponents points to the formation of spherulites with three-dimensional growth during primary crystallisation, while two-dimensional growth and more flattened structures are related to secondary crystallisation.

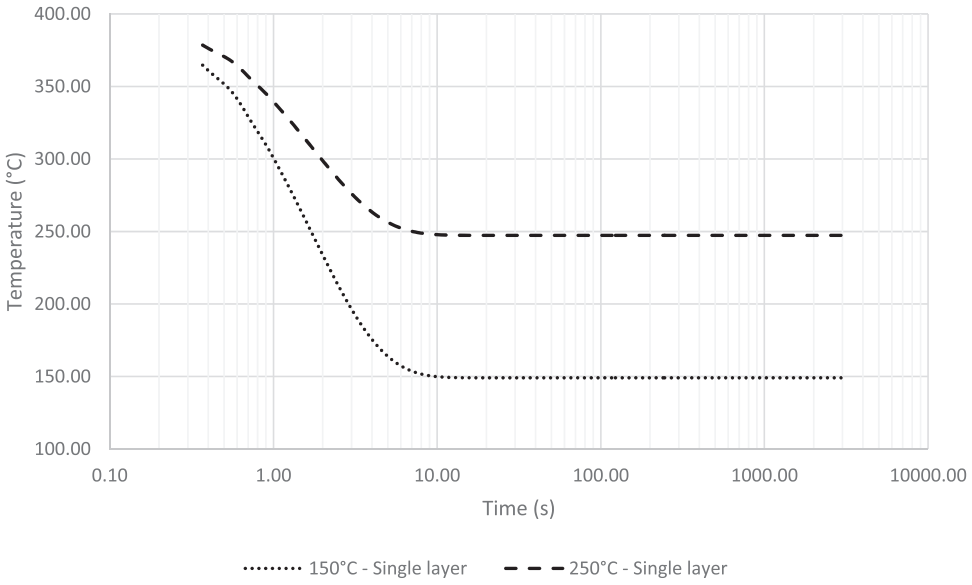

Fig. 14. Single layer thermal profiles generated for PEEK 450 G™ at 150 °C and 250 °C build surface temperature.

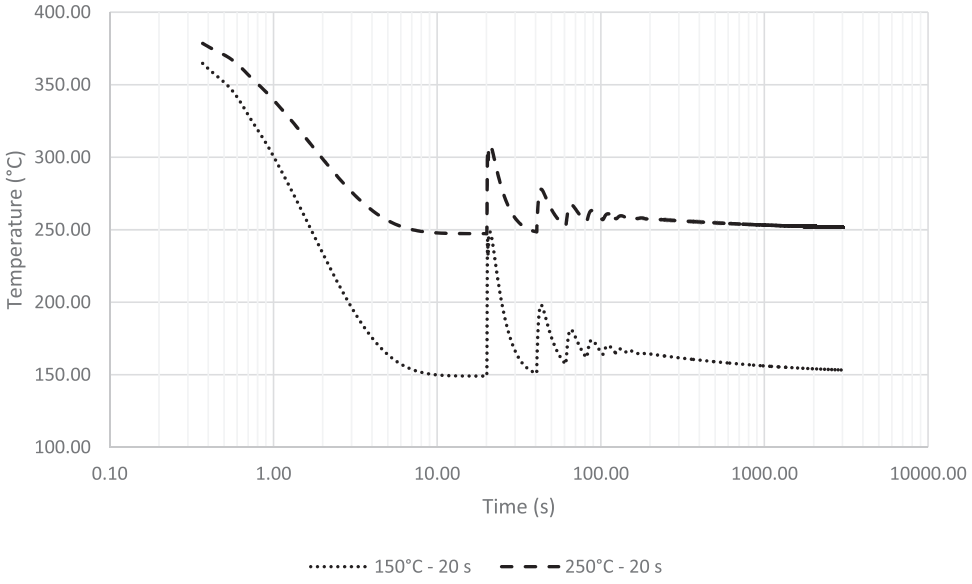

Fig. 15. Multiple layers of thermal profiles generated for PEEK 450 G™ at 150 °C and 250 °C build surface temperature.

It is interesting to note that in the fast crystallisation temperature range a V-shaped pattern is observed, especially in the exponents related to the secondary crystallisation (blue dots in Fig. 13). This indicates that crystallisation temperatures closer to 230 °C are more likely to create structures with lower three-dimensionality.

3.1.4. Profiles generated using the thermal model

The thermal profiles generated with the model proposed by C. Basgul et al. show clear differences when multiple layers are included. The single-layer thermal profiles show a rapid drop from the extrusion temperature to the build platform temperature. From the moment when the temperature of the extruded feedstock equals the temperature of the build platform, the temperature stabilizes, as shown in Fig. 14.

When multiple layers are included in the model, a series of peaks in layer temperature can be observed, each peak corresponding to the heat transmitted during the deposition of the subsequent layer, an effect that is dampened as more layers are added over the monitored layer. The phenomenon of crystallisation in such circumstances could be approximated, therefore, by a combination of a rapid decrease in temperature to the temperature of the build surface, at which a quasi-isothermal crystallisation takes place until the process is interrupted with a new layer added to the build surface, with the resulting temperature peak promoting the remelting of the previously deposited layer, as shown in Fig. 15.

After the remelting promoted by the subsequent layers, the temperature goes back to the build surface temperature and if new layers take long enough to be printed on top of the previous ones, the quasi-isothermal crystallisation starts over again. For the parameters selected in our analysis, it takes around 7 layers for the heat of subsequent layers to be almost fully dampened, however, this may vary according to the selected parameters, such as layer thickness or extrusion temperature.

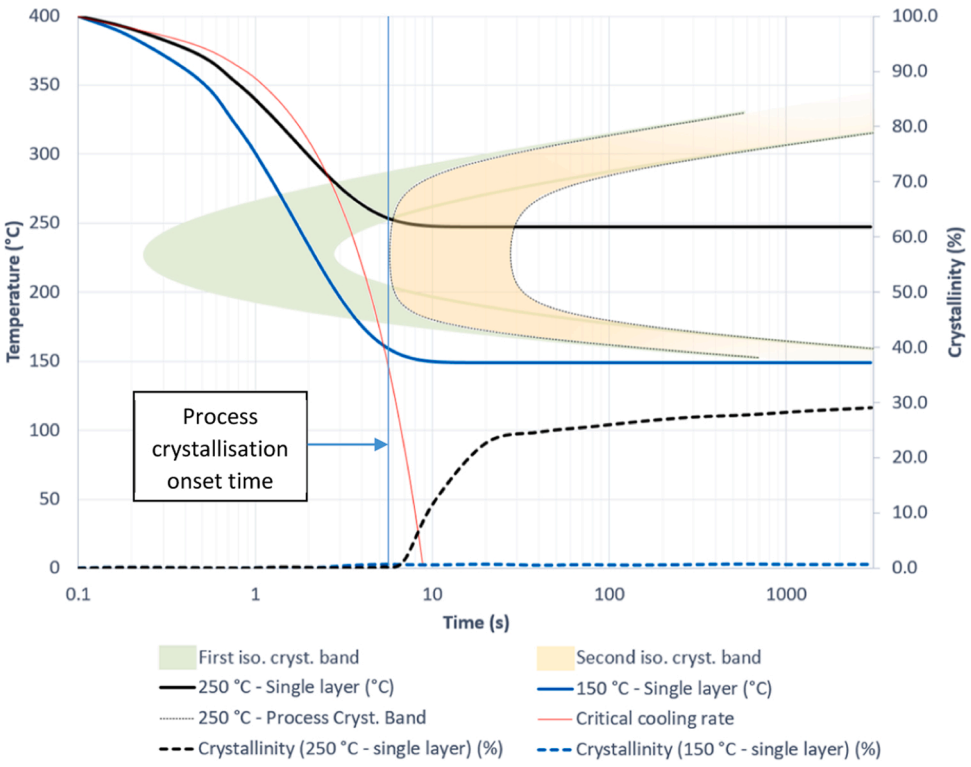

Fig. 16. Single layer crystallisation on MEX process for PEEK 450 G™ – Black and blue solid lines are the temperature of the simulated MEX thermal profile while black and blue dashed lines are the respective crystallinities. The red curve represents the critical cooling rate and the green and yellow regions are the crystallization bands.

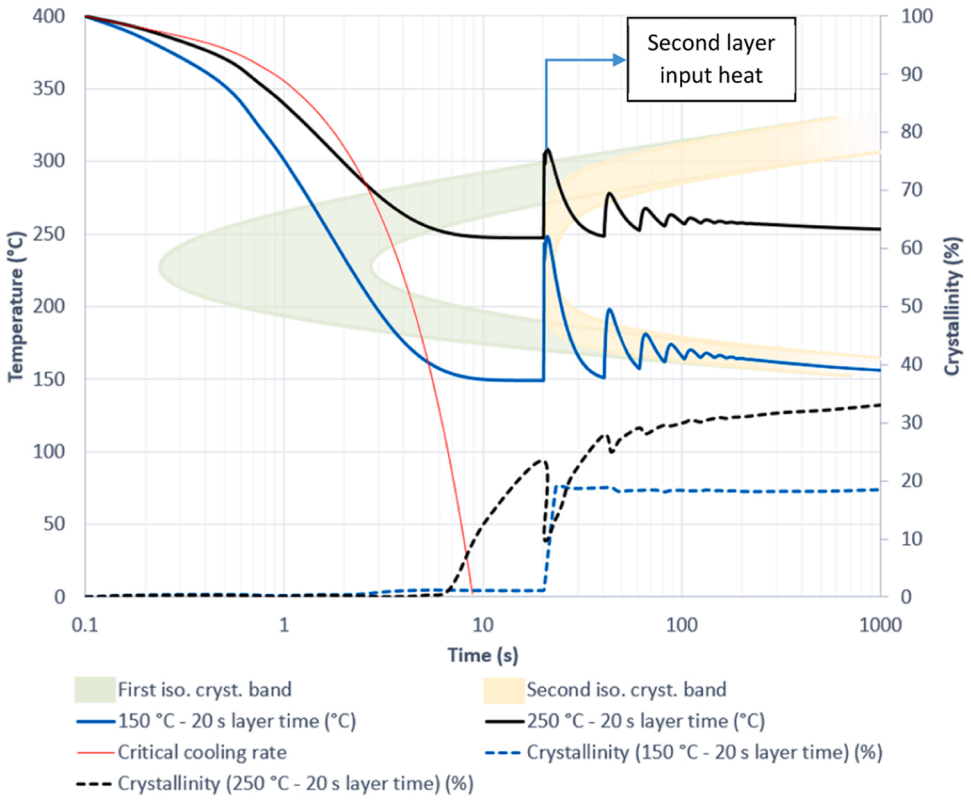

Fig. 17. Multiple layer crystallisation on MEX process for PEEK 450 G™ – 20 s layer time – Black and blue solid lines are the temperature of the simulated MEX thermal profile while black and blue dashed lines are the respective crystallinities. The red curve represents the critical cooling rate and the green and yellow regions are the crystallization bands.

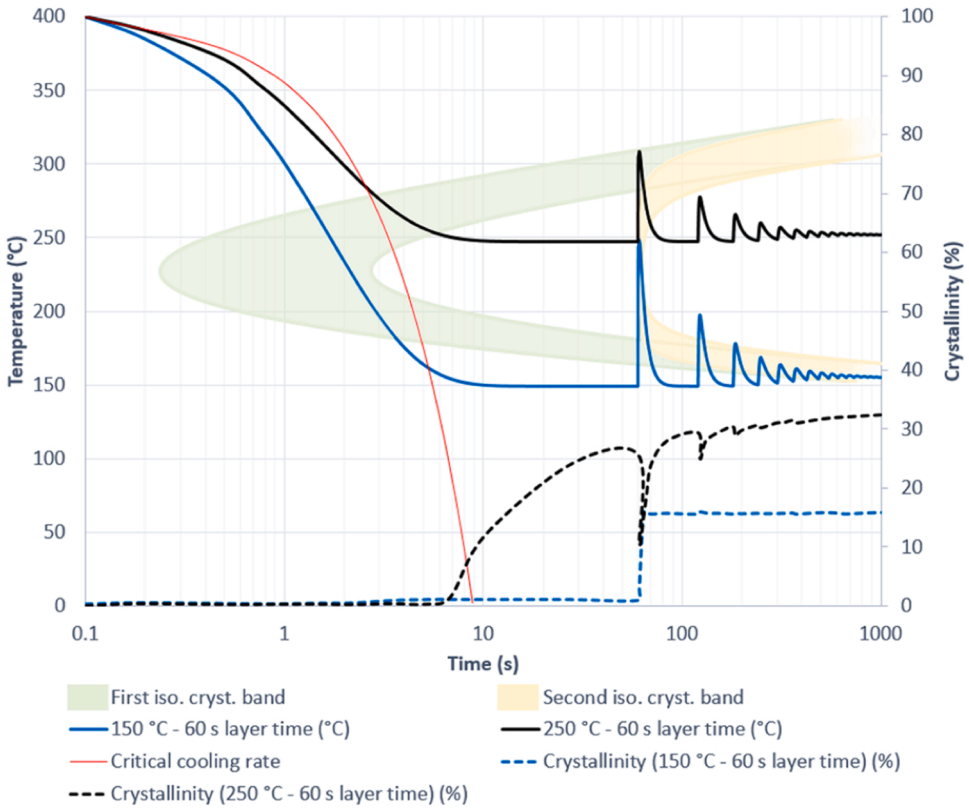

Fig. 18. Multiple layer crystallisation on MEX process for PEEK 450 G™ – 60 s layer time. – Black and blue solid lines are the temperatures of the simulated MEX thermal profile while black and blue dashed lines are the respective crystallinities. The red curve represents the critical cooling rate and the green and yellow regions are the crystallization bands.

Table A1
Cooling rates and target temperatures at which crystallinity values were measured for the non-isothermal crystallisation analysis.

Cooling rates (K s^{-1})	-45	-35	-30	-25	-20	-15	-10	-5	-4	-3.5	-3	-2.5	-2	-1.5	-1	-0.5
Target Temps (°C)	260.0	260.0	260.0	260.0	260.0	260.0	260.0	280.0	280.0	280.0	280.0	305.0	315.0	330.0	350.0	360.0
	250.0	250.0	250.0	250.0	250.0	250.0	255.0	275.0	275.0	275.0	275.0	280.0	305.0	320.0	290.0	300.0
	240.0	240.0	240.0	240.0	240.0	240.0	252.5	270.0	270.0	270.0	270.0	275.0	290.0	310.0	285.0	295.0
	230.0	230.0	230.0	230.0	230.0	230.0	250.0	265.0	265.0	265.0	265.0	270.0	285.0	300.0	282.5	292.5
	227.5	227.5	227.5	227.5	227.5	227.5	247.5	262.5	262.5	262.5	260.0	265.0	280.0	290.0	280.0	290.0
	225.0	225.0	225.0	225.0	225.0	225.0	245.0	260.0	260.0	260.0	257.5	262.5	275.0	280.0	277.5	287.5
	222.5	222.5	222.5	222.5	222.5	222.5	240.0	257.5	257.5	257.5	255.0	260.0	270.0	277.5	275.0	285.0
	220.0	220.0	220.0	220.0	220.0	220.0	235.0	255.0	255.0	255.0	252.5	257.5	265.0	275.0	272.5	282.5
	217.5	217.5	217.5	217.5	217.5	217.5	232.5	252.5	252.5	252.5	250.0	255.0	260.0	272.5	270.0	280.0
	215.0	215.0	215.0	215.0	215.0	215.0	230.0	250.0	250.0	250.0	245.0	250.0	255.0	270.0	267.5	277.5
	212.5	212.5	212.5	212.5	212.5	212.5	227.5	247.5	247.5	247.5	240.0	245.0	250.0	265.0	265.0	275.0
	210.0	210.0	210.0	210.0	210.0	210.0	225.0	245.0	245.0	245.0	235.0	240.0	245.0	260.0	262.5	272.5
	207.5	207.5	207.5	207.5	207.5	207.5	222.5	242.5	242.5	242.5	230.0	237.5	240.0	257.5	260.0	270.0
	205.0	205.0	205.0	205.0	205.0	205.0	220.0	240.0	240.0	240.0	227.5	230.0	235.0	255.0	255.0	265.0
	202.5	202.5	202.5	202.5	202.5	202.5	217.5	237.5	237.5	237.5	225.0	225.0	230.0	252.5	250.0	260.0
	200.0	200.0	200.0	200.0	200.0	200.0	215.0	235.0	235.0	235.0	222.5	220.0	225.0	250.0	240.0	250.0
	195.0	195.0	195.0	195.0	195.0	195.0	212.5	230.0	230.0	230.0	220.0	217.5	220.0	240.0	230.0	240.0
	190.0	190.0	190.0	190.0	190.0	190.0	210.0	220.0	220.0	220.0	215.0	215.0	215.0	190.0	220.0	230.0
	180.0	180.0	180.0	180.0	180.0	180.0	200.0	210.0	210.0	210.0	210.0	210.0	210.0	100.0	200.0	210.0

3.2. Crystallisation within the MEX process

3.2.1. Single-layer experiment

In Figs. 16, 17 and 18, the red line is the critical cooling rate. When cooling rates are higher than the critical cooling rate, the resulting crystallinity levels are lower than 0.7%, as observed in the evaluation of non-isothermal crystallisation.

In Fig. 16 it was found that the initial process cooling rates are slightly greater than the critical cooling rate, which could lead to a quenching of the material. This is confirmed by the very low crystallinity detected for the higher temperature (250 °C) and lower temperature (150 °C) up to the process crystallisation onset time.

For the higher build platform temperature, the process thermal profile crosses the critical cooling rate close to the green region, which is representative of the isothermal crystallisation band (0%–100% crystallinity). As the cooling rate is still high, the material is not crystallising as evidenced by the crystallinity measurements represented by the dotted lines. When the thermal profile reaches a quasi-isothermal regime, the crystallisation starts and the yellow region becomes the new isothermal crystallisation band.

For the lower temperature level (150 °C) the cooling rate is even higher. The material suffers a quenching process remaining outside the

green and yellow isothermal crystallisation regions and therefore the material remains amorphous.

3.2.2. Multiple layer experiment

For the multiple-layer experiment, the initial crystallisation behaviour was similar to that observed in the single-layer experiment, however, the process is extensively affected by the heat provided by the subsequent layers. Both return times tested, 20 s and 60 s, are shown in Figs. 17 and 18.

For both return times, crystallinity growth was detected, however, for the lower build platform temperature it just appears after the second layer deposition, which is represented in the thermal profile by the first temperature peak after the material reaches the build platform temperature. The second layer promotes an input heat which can cause an increase in temperature beyond the upper boundary of the crystallisation region in the TTT chart, even if for a brief moment.

For the higher temperature level (250 °C), a rapid crystallinity drop followed by a rebound of the crystallisation process was observed during the second layer deposition, the same effect is present to a lesser extent for the following layers. As soon as the temperature drops again, crystallisation resumes, however, as the remelting may be incomplete, the crystallisation process reaches the previous crystallinity level faster, happening inside a shorter secondary crystallisation band.

The crystalline phase developed before the input heat by the subsequent layers was partially remelted during the second layer deposition, being reduced by around 58% for the 20 s return time (from approximately 24% to 10%) and around 65% for the 60 s return time (from approximately 28% to 10%).

For the lower build platform temperature, the extra heat provided by the subsequent layers promoted a cold-crystallisation of the build surface. At this temperature level (150 °C) the crystallisation was practically absent before the second layer deposition, however, during the second layer deposition, the crystallinity jumps from ~0% to approximately 19% (for 20 s return time) and 16% (for 60 s return time). This effect is explained by the greater mobility and rearrangement capacity of the polymeric chains, promoted by the heat added to the build surface during the subsequent layer deposition.

When evaluating the effect of layer time based on crystallinity measurement for the 60 s layer time (Fig. 18) and comparing it with the 20 s (Fig. 17), it was found that shorter layer times slightly increased the crystallisation rate, both for the lower and higher temperatures levels. The increase in the return time reduces the resulting crystallinity levels, probably because it affects the polymeric chain entanglement before the input heat by the subsequent layers.

When comparing the results from the multiple layer experiment with the crystallisation on the single-layer experiment, the crystallisation rate for the multiple layer processes is higher, surpassing the 30% crystallinity level around 200 s for both return times, a much shorter time when compared to the single-layer process, which was still below 30% even after 3000 s. This finding suggests an extra boost in the crystallisation provided by shorter layer times and layer remelting.

4. Conclusions

Isothermal and non-isothermal crystallisation analysis of PEEK 450 G™ was successfully carried out by combining DSC and FSC techniques in addition to simulated in-process crystallisation measurements. Real-time measurement or modelling of the crystallisation during printing in the MEX process can become a complex task, since the process is based on the superposition of multiple layers that exert thermal influence on the predecessor layers, it is natural that temperature variations are rapid and frequent, such as observed in the thermal profiles.

However, with the use of the FSC technique, it was possible to replicate the thermal profiles with good accuracy and measure the crystallinity at any point as a function of time, which can be very useful for understanding geometric distortions related to the crystallization process. The profiles obtained through the simulation were simplified and the crystallinity of each point was successfully measured and compared with the expected crystallinity in a constant temperature crystallisation scenario, as predicted by the TTT chart. This approach proved to be useful and provided several insights into the process of crystallisation dynamics.

It was found that the higher the temperature reached during the remelting peak, the greater the remelting of the crystalline phase of the build surface, which should result in greater mobility of polymeric chains, improving interlayer entanglement and mechanical properties, especially in the Z direction.

For the first layers, if the extrusion temperature remains constant, the maximum temperature of the remelting peak will be greatly influenced by the build platform temperature. For layers further away from the build platform, the build room temperature becomes more important, due to a lower influence from the build platform, which suggests that to obtain homogeneous parts, a good approach could be to have systems with higher build room temperatures, able to guarantee adequate build surface remelting and subsequent layer adhesion. This conclusion is valid for fast crystallizing polymers such as PEEK 450 G™ and may follow a slightly different trend for slower crystallizing PAEKs.

CRediT authorship contribution statement

Cleiton André Comelli: Writing – review & editing, Writing – original draft, Methodology, Investigation, Formal analysis, Data curation, Conceptualization. **Nan Yi:** Writing – review & editing, Investigation. **Richard Davies:** Supervision. **HenkJan van der Pol:** Validation, Supervision, Project administration, Funding acquisition. **Oana Ghita:** Writing – review & editing, Validation, Supervision, Project administration, Funding acquisition, Data curation.

Declaration of Competing Interest

The authors declare that they have no known competing financial interests or personal relationships that could have appeared to influence the work reported in this paper.

Data Availability

Data will be made available on request.

Acknowledgements

This work was supported by Bond3D High Performance 3D Technology BV and the University of Exeter.

Appendix A

see.Table A1.

References

[1] Victrex, “Victrex PEEK 450G,” PEEK 450G technical data sheet, 2019. [Online]. Available: https://www.victrex.com/-/media/downloads/datasheets/victrex_tds_450g.pdf.
[2] M.T. Bishop, F.E. Karasz, P.S. Russo, K.H. Langley, Solubility and properties of a poly(aryl ether ketone) in strong acids, Macromolecules vol. 18 (1985) 86–93.
[3] A.R. Zanjanijam, I. Major, J.G. Lyons, U. Lafont, D.M. Devine, Fused filament fabrication of peek: A review of process-structure-property relationships, Polym. (Basel). vol. 12 (8) (2020) 29.
[4] C.T.S. Uk, “Mechanical properties of poly(ether-ether- ketone) for engineering applications,” vol. 26, pp. 1385–1393.
[5] S. Tan, A. Su, J. Luo, E. Zhou, Crystallization kinetics of poly (ether ether ketone) (PEEK) from its metastable melt, Polymer vol. 40 (1999) 1223–1231.
[6] ASTM International, “Standard Terminology for Additive Manufacturing – General Principles – Terminology.” ISO/ASTM International 2015, p. 19, 2015.
[7] L. Lin et al., Additive manufacturing of complex-shaped and high-performance aluminum nitride-based components for thermal management Addit. Manuf., vol. 52, no. September 2021, p. 102671, 2022.

[8] A. El Magri, K. El Mabrouk, S. Vaudreuil, H. Chibane, M.E. Touhami, Optimization of printing parameters for improvement of mechanical and thermal performances of 3D printed poly(ether ether ketone) parts, J. Appl. Polym. Sci. vol. 137 (37) (2020) 1–14.
[9] R. Rahman, Kazi Moshiur; Letcher, Todd; Reese, Mechanical properties of additively manufactured peek components using fused filament fabrication Proc. ASME 2015 Int. Mech. Eng. Congr. Expo., pp. 1–11, 2015.
[10] M.F. Arif, S. Kumar, K.M. Varadarajan, W.J. Cantwell, Performance of biocompatible PEEK processed by fused deposition additive manufacturing, Mater. Des. vol. 146 (2018) 249–259.
[11] S. Berretta, K.E. Evans, O. Ghita, Processability of PEEK, a new polymer for high temperature laser sintering (HT-LS), Eur. Polym. J. vol. 68 (2015) 243–266.
[12] D. Popescu, A. Zapciu, C. Amza, F. Baciu, R. Marinescu, FDM process parameters influence over the mechanical properties of polymer specimens: a review, Polym. Test. vol. 69 (April) (2018) 157–166.
[13] E. Harkin-jones, M. Wegrzyn, P.K. Sharma, A. Zhigunov, Improvement of the layer-layer adhesion in FFF 3D printed PEEK / carbon fibre composites, no vol. 149 (2021).
[14] J. Zheng, et al., Additively-manufactured PEEK / HA porous scaffolds with excellent osteogenesis for bone tissue repairing, Compos. Part B vol. 232 (November 2021) (2022), 109508.
[15] A. Patel, M. Taufik, Materials today: proceedings nanocomposite materials for fused filament fabrication, Mater. Today Proc. vol. 47 (2021) 5142–5150.
[16] B. Valentan, T. Brajlih, A. Anderson, I. Drstven, Processing Poly (Ether Etherketone) on a 3D Printer for Thermoplastic Modelling, Mater. Tehnol. vol. 47 (6) (2013) 715–721.
[17] N. Yi, R. Davies, A. Chaplin, P. Mccutchion, O. Ghita, Slow and fast crystallising poly aryl ether ketones (PAEKs) in 3D printing: Crystallisation kinetics, morphology, and mechanical properties, Addit. Manuf. vol. 39 (December 2020) (2021), 101843.
[18] D. Zeng, M. Rebandt, G. Lacaria, E. Lee, X. Su, Numerical simulation of the temperature history for plastic parts in fused filament fabrication (FFF) process, Mater. Sci. (2019) 1230–1241.
[19] D. Vaes, P. Van Puyvelde, Semi-crystalline feedstock for filament-based 3D printing of polymers, Prog. Polym. Sci. vol. 118 (May) (2021), 101411.
[20] D. Vaes, M. Coppens, B. Goderis, W. Zoetelief, P. Van Puyvelde, The extent of interlayer bond strength during fused filament fabrication of nylon copolymers: an interplay between thermal history and crystalline morphology, Polym. (Basel) vol. 13 (16) (2021).
[21] D. Vaes, P. Van Puyvelde, Semi-crystalline feedstock for filament-based 3D printing of polymers, Prog. Polym. Sci. vol. 118 (2021), 101411.
[22] D.C. Bassett, R.H. Olley, I.A.M. Al Raheil, On crystallization phenomena in PEEK, Polymer vol. 29 (10) (1988) 1745–1754.
[23] L. Jin, J. Ball, T. Bremner, H. Sue, Crystallization behavior and morphological characterization of poly (ether ether ketone), Polym. (Guildf.) vol. 55 (20) (2014) 5255–5265.
[24] J. Seo, et al., Isothermal crystallization of poly (ether ether ketone) with different molecular weights over a wide temperature range, Polym. Cryst. (August 2018) (2019) 12.
[25] P. Cebe, Non-isothermal crystallization of poly(etheretherketone) aromatic polymer composite, Polym. Compos. vol. 9 (4) (1988) 271–279.
[26] X. Tardif, et al., Experimental study of crystallization of PolyEtherEtherKetone (PEEK) over a large temperature range using a nano-calorimeter, Polym. Test. vol. 36 (2014) 10–19.
[27] T. Liu, Z. Mo, S. Wang, H. Zhang, Nonisothermal melt and cold crystallization kinetics of poly(aryl ether ether ketone ketone), Polym. Eng. Sci. vol. 37 (3) (. 1997) 568–575.
[28] P. Cebe, S.-D. Hong, Crystallization behaviour of poly(ether-ether-ketone), Polymer vol. 27 (8) (1986) 1183–1192.
[29] C. Bas, A.C. Grillet, F. Thimon, N.D. Albérola, Crystallization kinetics of poly(aryl ether ether ketone): time-temperature-transformation and continuous-cooling-transformation diagrams, Eur. Polym. J. vol. 31 (10) (1995) 911–921.
[30] J.J.C. Cruz-Pinto, J.A. Martins, M.J. Oliveira, The isothermal crystallization of engineering polymers - POM and PEEK, Colloid Polym. Sci. vol. 16 (May 1991) (1994) 1–16.
[31] P.J. Phillips, "Bulk Crystallization of Poly(Ary1 Ether Ether Ketone) (PEEK)," vol. 3, no. 5.
[32] C. Basgul, F.M. Thieringer, S.M. Kurtz, Heat transfer-based non-isothermal healing model for the interfacial bonding strength of fused filament fabricated polyetheretherketone, Addit. Manuf. vol. 46 (June) (2021), 102097.
[33] D. Vaes, M. Coppens, B. Goderis, W. Zoetelief, P. Van Puyvelde, P. Van Puyvelde, Assessment of crystallinity development during fused filament fabrication through fast scanning, Appl. Sci. vol. 9 (13) (2019) 1–20.
[34] A. Lepoivre, N. Boyard, A. Levy, V. Sobotka, Heat transfer and adhesion study for the FFF additive manufacturing process, Procedia Manuf. vol. 47 (2019) (2020) 948–955.
[35] Q. Sun, G.M. Rizvi, C.T. Bellehumeur, P. Gu, Effect of processing conditions on the bonding quality of FDM polymer filaments, Rapid Prototyp. J. vol. 14 (2) (2008) 72–80.
[36] H.R. Vanaei, A comparative in-process monitoring of temperature profile in fused filament fabrication, Polym. Eng. Sci. (2021) 68–76.
[37] T. Tichý, O. Šefl, P. Veselý, K. Dušek, D. Bušek, Mathematical modelling of temperature distribution in selected parts of fff printer during 3d printing process, Polym. (Basel) vol. 13 (23) (2021) 1–10.
[38] N. Schiavone, V. Verney, and H. Askanian, "Effect of 3D Printing Temperature Profile on Polymer Materials Behavior," vol. 00, no. 00, pp. 1–15, 2020.
[39] G. Vanden, P. Daniel, Performance and calibration of the Flash DSC 1, a new, MEMS-Based fast Scanning Calor. (2012) 1533–1546.
[40] C.N. Velisaris, J.C. Seferis, Crystallization kinetics of polyetheretherketone (PEEK) matrices, Polym. Eng. Sci. vol. 26 (22) (1986) 1574–1581.